Shap. Mem. Superelasticity
https://doi.org/10.1007/s40830-024-00478-w

ORIGINAL RESEARCH ARTICLE

Atomistic Simulation of the Effect of H-Phase Precipitate on the Transformation Temperatures and Stress-Induced Phase Transformation in Ni-Rich NiTiHf

Saeed Ataollahi[1] · Mohammad J. Mahtabi[1]

Received: 26 October 2023 / Revised: 20 January 2024 / Accepted: 28 February 2024

Abstract Precipitation hardening is considered the most feasible method for strengthening NiTiHf alloys. In order to design the optimum aging treatment to form precipitates, it is crucial to understand the effect of precipitates on the thermomechanical behavior of these alloys. In this research, the effect of H-phase precipitates was studied on the martensitic and superelastic behavior of Ni-rich NiTiHf. Using atomistic simulations, two scenarios for formation of precipitates, resembling the short and long aging time of the alloy, were considered. In the first case a single and large precipitate was embedded into the center of NiTiHf matrix, and in the second case eight fine precipitates were inserted into the model. Upon the calculation of the transformation temperatures, the models with precipitates showed higher austenite start and finish temperatures. Moreover, by simulating the stress-induced phase transformation, it was found that the presence of fine precipitates inhibits the formation of different martensite variants leading to smaller transformation strains.

Keywords H-phase · Superelasticity · NiTiHf · High-temperature shape memory alloy · Molecular dynamics

Introduction

Applications of high-temperature shape memory alloys (HTSMAs) may encounter serious challenges such as unstable cyclic behavior and large plastic deformations at high stress and temperature [1, 2]. There are a few approaches such as thermomechanical processing, solid solution hardening, and precipitation hardening that can be employed to overcome these challenges and improve the shape memory and mechanical properties of HTSMAs [3–6]. However, since the HTSMAs are often ordered intermetallics with limited ductility at low and intermediate temperatures, applying thermomechanical processing can be difficult and expensive [7]. Therefore, precipitation hardening is considered the most practical and cost-effective method among other strengthening approaches. Introducing nanoscale precipitates into the material can increase the critical shear stress required for slip in the matrix, resulting in improved shape memory properties [8]. In addition, the inclusion of these nanoparticles can act as barrier against dislocation motion leading to enhanced fatigue life and cyclic stability [8–10].

Among the HTSMAs, NiTi-based alloys have been studied the most since they exhibit the highest transformation temperatures (TTs). There are a limited set of elements, including Pt, Pd, Au and Hf, which can be employed for alloying with NiTi to create ternary and quaternary HTSMAs [11–13]. It has been reported that the addition of a similar content of Hf has a more significant effect on the TTs in comparison with Pd and Au [1, 4]. Furthermore, unlike NiTiAu, NiTiPd and NiTiPt which are limited to high priority applications due to being expensive, NiTiHf alloys can be employed in a broad range of high-temperature applications [14–16]. Additionally, NiTiHf exhibits superior transformation strains compared to NiTi in both tension and compression. Adding even minor quantities of Hf to NiTi improves the transformation characteristics. Under compression, NiTiHf alloys can achieve transformation strains of up to 7%, and under tension, these strains can reach up to 15%, while those values for binary NiTi alloys are 5.5% in compression and 10% in tension [17].

✉ Mohammad J. Mahtabi
Mohammad-Mahtabi@utc.edu; mjmahtabi@gmail.com

[1] Department of Mechanical Engineering, The University of Tennessee at Chattanooga, Chattanooga, TN, USA

Published online: 19 March 2024

Based on previous studies, it has been found that NiTiHf alloys can contain different types of precipitates, which are influenced by several factors such as alloy composition—specifically whether it is Ti-rich or Ni-rich—and heat-treatment schedule, among others. For instance, König et al. [18] investigated a wide range of Ti-rich compositions by fabricating thin films of NiTiHf and observed four distinct types of precipitate, i.e., HfNi(Ti), Ti_2Ni(Hf), Hf_2Ni(Ti), and the Laves phase. Their findings demonstrated that with an increase in the Ti content within the NiTiHf alloy, there was a concurrent rise in the occurrence of the secondary Laves phase. The Ti_2Ni(Hf) precipitates have also been observed in Ni-lean NiTiHf alloys [19, 20]. It has been reported that increasing the Ni content decreases the volume fraction of Ti_2Ni(Hf) precipitates, however, they can still be found in slightly Ni-rich compositions [19, 21]. Fine Ti_2Ni(Hf) precipitates act as vital agents in strengthening and improving the shape memory and superelasticity properties of NiTiHf alloys. It should be noted that the size of the Ti_2Ni(Hf) precipitates significantly influences and controls the patterns of martensite.

The characterization of precipitate phase in Ni-rich NiTiHf was performed by Han et al. [22] where they conducted an aging heat treatment at 600 °C for 150 h on $Ni_{48.5}Ti_{36.5}Hf_{15}$ alloy. By performing comprehensive Transmission Electron Microscopy (TEM) analyses, they identified the presence of a specific type of precipitate in the alloy with an approximate composition of $Ti_{0.6}Hf_{0.4}Ni$. This precipitate exhibited a face-centered orthorhombic lattice structure and demonstrated a close association with the B2-type matrix. Furthermore, the precipitate possessed a distinct oblate spindle-like shape, which was then called the "H-phase" precipitate. To identify the exact composition of the precipitate, Yang et al. [23] utilized advanced techniques such as high-angle annular dark-field scanning transmission electron microscopy (HAADF-STEM), atom probe tomography (APT), and first-principles calculations. They subjected an alloy with a composition of $Ni_{50.3}Ti_{29.7}Hf_{20}$ to an aging process at 600 °C for 815 h. By extending the aging time, the H-phase precipitates coarsened, which facilitated the precise characterization of them. Upon examination, it was revealed that the formed H-phase precipitate possessed *F 2/d 2/d 2/d* space group with a composition of Ni_3TiHf_2. Nonetheless, it is essential to emphasize that both prior research [24–26] and the observations made by Yang et al. [23] have demonstrated that the composition of H-phase precipitates can differ depending on the initial alloy's composition, even when subjected to similar heat treatment processes. This is in contrast to Ni_4Ti_3 precipitates, which form with a fixed composition regardless of the initial composition of NiTi.

It is important to highlight that the effectiveness of the strengthening achieved by precipitates depends on various factors, including their size, volume fraction, interparticle spacing, and coherency with the matrix [27]. Additionally, factors such as aging time, temperature, and lattice mismatch between the matrix and precipitates introduce local stress fields that can modify the strengthening behavior, martensite nucleation, and shape memory properties. In spite of many variables involved in the alloy design by precipitation, limited research has been conducted to investigate the influence of precipitates on the behavior of NiTiHf alloys. To gain further understanding of the properties of alloys, atomistic simulations are considered a viable and cost-effective method to explore the microstructural features of the precipitates in NiTiHf [28]. In this study, molecular dynamics (MD) simulations were employed to investigate the effect of precipitates on the temperature- and stress-induced phase transformation behaviors of Ni-rich NiTiHf Alloy. Additionally, direction-dependence of superelastic and martensitic response of NiTiHf models was studied by applying compressive stress in various crystallographic directions of the models containing one or more precipitates.

Computational Method

In order to simulate the effect of H-phase precipitate on the temperature- and stress-induced phase transformation of NiTiHf, MD simulations were employed. To describe the interaction of atoms in the ternary alloy, a newly developed 2NN MEAM potential for NiTiHf was used [29]. It has been shown that the computed lattice parameters of NiTiHf with varying compositions for both cubic B2 (austenite) and monoclinic B19′ (martensite) structures closely agree with experimental values when employing the specified interatomic potential. Additionally, this potential has effectively replicated the high-temperature superelastic and low-temperature martensitic behavior of Ni-rich NiTiHf in prior simulations [29]. LAMMPS [30] and Ovito [31] packages were utilized for MD simulations and visualization of results, respectively. For the atomic arrangement, models of B2 crystal structure of a widely used Ni-rich composition, i.e., $Ni_{50.3}Ti_{29.7}Hf_{20}$, were generated using Atomsk [32]. To generate NiTiHf models with the desired composition, an equiatomic NiTi system was created. Subsequently, Hf atoms were introduced into the system and replaced by Ti atoms in quantities that matched the desired final composition. This introduction of Hf atoms was done randomly. Finally, the distribution of atoms was visually examined to verify that there were no clusters or blocks of Hf atoms, ensuring a uniform dispersion of Hf throughout the model. According to the crystal structure reported by Yang et al. [23] for Ni-rich NiTiHf, spindle-shaped H-phase precipitates were modeled of Ni_3TiHf_2 composition and an orthorhombic structure. It is known that shorter aging time at a lower temperature leads to formation of fine and coherent H-phase

precipitates. In contrast, at elevated aging temperatures and longer time, precipitates grow, resulting in increased interparticle distances. To investigate the influence of each of these cases, two scenarios were examined for models containing precipitates. In the first scenario, the model featured a single, large precipitate positioned at the center of the matrix, corresponding to an alloy subjected to longer aging. Conversely, in the second scenario, a model of the same size consisted of eight smaller precipitates evenly dispersed within each of the octants of the box. The percentage of precipitation was similar in both scenarios.

In order to model NiTiHf matrix with one precipitate (referred to as single-precipitate model), the oblate spindle-like precipitate was embedded into the center of a NiTiHf cube with $250\times250\times250$ Å dimensions. The lattice correspondence of the precipitate (subscript H) to the matrix (subscript B2) was: $[100]_H \rightarrow [001]_{B2}$; $[010]_H \rightarrow [110]_{B2}$; $[001]_H \rightarrow \left[\bar{1}10\right]_{B2}$. Moreover, the minor axis of the precipitate was along [001] orientation of the matrix. For the other scenario with multiple precipitates (referred to as multi-precipitate model), first a similar procedure was employed on a smaller model with $125\times125\times125$ Å dimensions, and a proportionally smaller precipitate was embedded into the center of the model. Then, this model was replicated consecutively in all the three dimensions, to generate the final model with eight precipitates. In both scenarios, the models contained almost one million atoms and the fraction of the precipitates was 2.6%. The aspect ratios (the ratio of major to minor axis length) of precipitates were based on the experiments of Evirgen et al. [33].The details of the dimensions and the crystal structure of the modeled precipitates are presented in Table 1. In addition, Fig. 1a shows the single-precipitate model (cut in the middle for better visualization) and Fig. 1b presents the distribution of the fine precipitates in the multi-precipitate model (matrix atoms are not shown). It should be noted that for comparison purposes, in this study the precipitate arrangement was considered to be the same and parallel in both single-precipitate and multi-precipitate models. More cases will be considered in the future for the cases of intersecting precipitates as reported by [34]. During the simulation, periodic boundary conditions were applied to the models in all the three dimensions and the timestep was taken as 2 fs. To control the temperature and pressure, Nose–Hoover thermostating and barostating were applied on all atoms.

Temperature-Induced Phase Transformation

To capture the effect of H-phase precipitates on the temperature-induced phase transformation of NiTiHf, a cycle of cooling followed by heating was applied to models with and without precipitates. Before applying the thermal cycle, the models were equilibrated at 800 °C to obtain similar initial condition of austenite. Following equilibration, the models were cooled down from 800 to 0 °C and then heated back to 800 °C at a constant rate of 2.75 °C/ps. The rate of martensitic transformation (computed through measuring the martensite fraction in the model in each step) during thermal cycle was extracted for all models, where its variation has been presented in Fig. 2a with respect to the temperature change. In these graphs, the sudden jump in the rate of martensitic transformation during cooling indicates the start of

Table 1 Details of the modeled orthorhombic precipitates

Shape	Crystal structure	Major axis (Å)		Minor axis (Å)		Lattice parameters of the precipitate			
		Single	Multi	Single	Multi	a (Å)	b (Å)	c (Å)	$\alpha=\beta=\gamma$ (°)
Oblate spindle	Ni_3TiHf_3	150	70	50	22	12.66	8.83	26.14	90

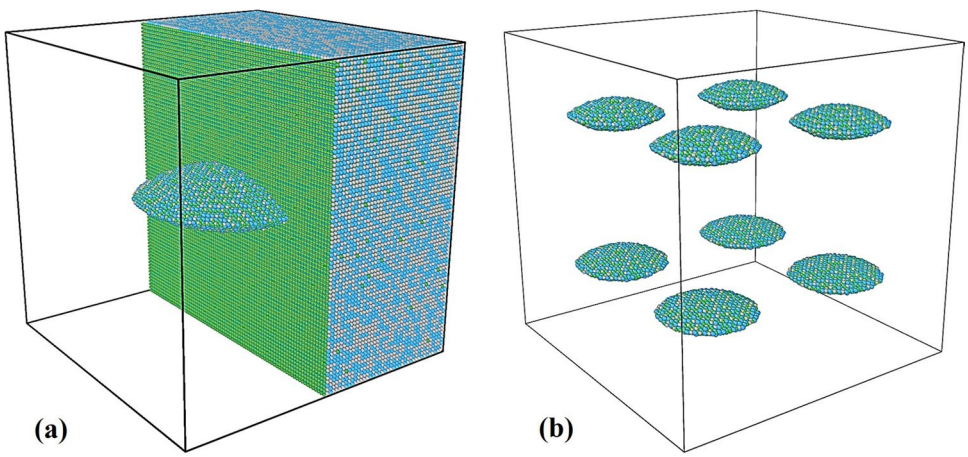

Fig. 1 **a** Single-precipitate model (cut in the middle for better visualization), **b** distribution of fine precipitates in multi-precipitate model (matrix atoms are not shown)

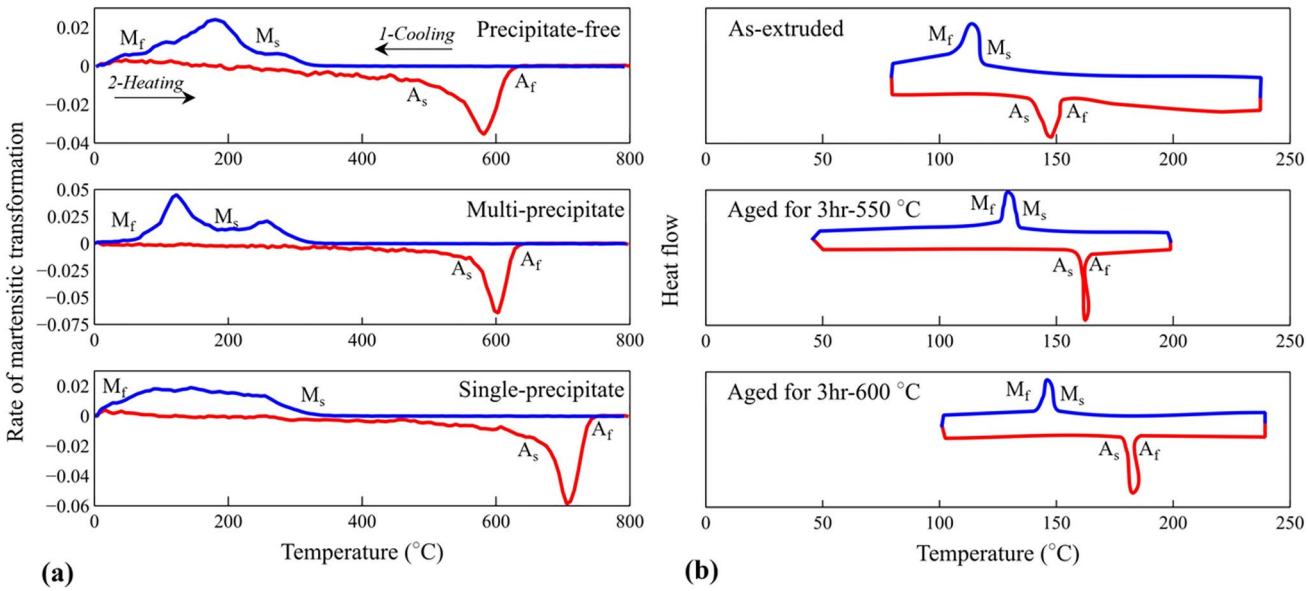

Fig. 2 **a** Variation of the rate of martensitic transformation with temperature change, indicating the transformation temperatures of the material, **b** DSC curves of $Ni_{50.3}Ti_{29.7}Hf_{20}$ obtained from experiments for different aging conditions [36]

transformation from austenite to martensite (thus, martensite start temperature, M_s) and the end of subsequent drop in the rate of transformation indicates the completion of martensitic transformation (thus martensite finish temperature, M_f). Similarly, the sudden changes in the rate of transformation during heating are the indication of martensite to austenite transformation, A_s, austenite start and A_f, austenite finish temperatures. It can be seen that the A_s and A_f increased in the models that contained precipitate compared to the precipitate-free model. While the extent of this change is significant for the single-precipitate model, the multi-precipitate model showed a lower increase. Karaca et al. [35] also reported the same trend of change in the TTs, by conducting heat treatment at different temperatures on $Ni_{50.3}Ti_{29.7}Hf_{20}$ alloy. Based on the Differential Scanning Calorimetry (DSC) curves of their experiments (Fig. 2b [35]), aged samples showed higher TTs as opposed to as-extruded sample that exhibited the lowest TTs. Among heat-treated samples, the ones that aged at higher temperature formed larger precipitates leading to yet higher TTs.

It should be noted that the composition difference between the matrix and the precipitate can change the overall composition of the model compared to the initially stated composition. This could be a potential reason for the difference of TTs among various models. Table 2 shows the overall compositions of the final state of different models. As can be seen in this table, the overall composition across different models will remain close to the intended composition. On the other hand, the small difference between the TTs of multi-precipitate and precipitate-free models suggests that the composition change cannot be considered the main

Table 2 Final composition of the models after adding the precipitate(s)

	Ni	Ti	Hf
Precipitate-free	50.3	29.7	20
Single-precipitate	50.3	29.4	20.3
Multi-precipitate	50.3	29.4	20.3

reason for the increase in the TTs of the single-precipitate model. To investigate the difference between TTs of precipitated and precipitate-free models, a cross-section of each model showing the present austenite and martensite phases at the end of cooling are presented in Fig. 3. Color coding based on Polyhedral template matching (PTM) algorithm [37] was employed to identify different phases in each of the models. In Fig. 3, the martensite phase (B19′ structure) is shown as red, and the austenite phase (B2 structure) is presented as blue. As can be seen in this figure, in all the models most of the initially austenite material has undergone phase transformation into martensite. However, the blue bands of atoms, which signify the twinning planes, distributed densely in the precipitate-free model, whereas in the single-precipitate model these bands are lumped into a large area. It should be noted that during the reverse phase transformation from martensite to austenite, these twinning planes act as nucleation zones for austenite. Therefore, the reverse transformation from martensite to austenite during heating occurs sooner (i.e., at a lower temperature) in the precipitate-free model, leading to lower A_s and A_f. Conversely, in the single-precipitate model, which only exhibits one rather

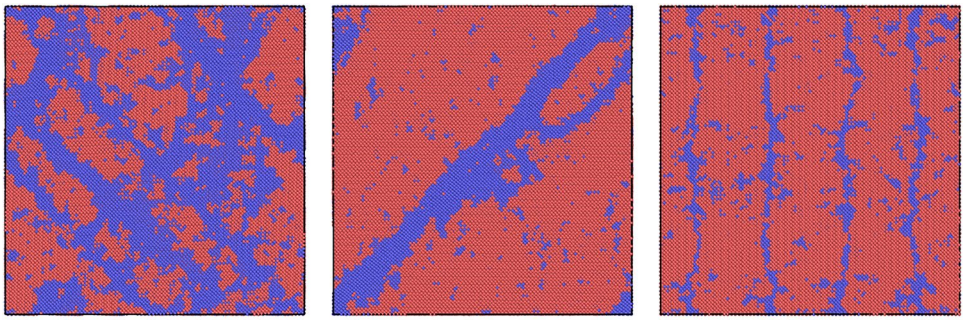

(a) Precipitate-free (b) Single-precipitate (c) Multi-precipitate

Fig. 3 Present austenite and martensite phases at the end of cooling in different models (red and blue regions denote martensite and austenite phases, respectively) (Color figure online)

thick twinning plane, due to the existence of smaller potential nucleation zones, the reverse phase transformation happens at a higher temperature and, thus, higher A_s and A_f will be observed for this case. In the multi-precipitate model, the number of twinning planes is larger than the single-precipitate model, yet less than the precipitate-free model, which accordingly results in significantly lower TTs compared to the single-precipitate model, and slightly higher TTs than the precipitate-free model.

Stress-Induced Phase Transformation

In order to analyze how the presence of precipitates affects the superelastic and martensitic responses of NiTiHf alloy, a compressive stress was applied to the aforementioned precipitated and precipitate-free models at two temperatures: one below M_f and one above A_f. The temperature above A_f for superelastic behavior was chosen in a way that the resulting stress–strain responses could be compared. Since according to the Clausius–Clapeyron equation there is a linear relationship between transformation stress and temperature, stress-induced phase transformation was studied at $A_f + 50$ °C for each model. Hence, using an isobaric-isothermal NPT ensemble, the models were equilibrated and loaded at 0 °C as a martensitic temperature. Using the same procedure, the precipitate-free, single-precipitate, and multi-precipitate models were subjected to equilibration and loading at 675, 780, and 685 °C (as austenitic temperatures), respectively. These temperatures were obtained according to the TTs in Fig. 2. A uniaxial compressive load was gradually applied along the [100] direction from 0 to 2 GPa, followed by unloading of the model back to 0 GPa. Before studying the NiTiHf models, an equivalent model composed solely of the precipitate (a box with the crystal structure of the precipitate, Ni_3TiHf_2) was analyzed. This preliminary investigation aimed to gain insight into the stress–strain behavior of the precipitate. Figure 4 presents the stress–strain response of the precipitate at 0 °C and 675 °C. As can be seen in Fig. 4a at 0 °C, the model reaches more than 0.03 strain with a residual strain of 0.01 at the end of unloading. Furthermore, an

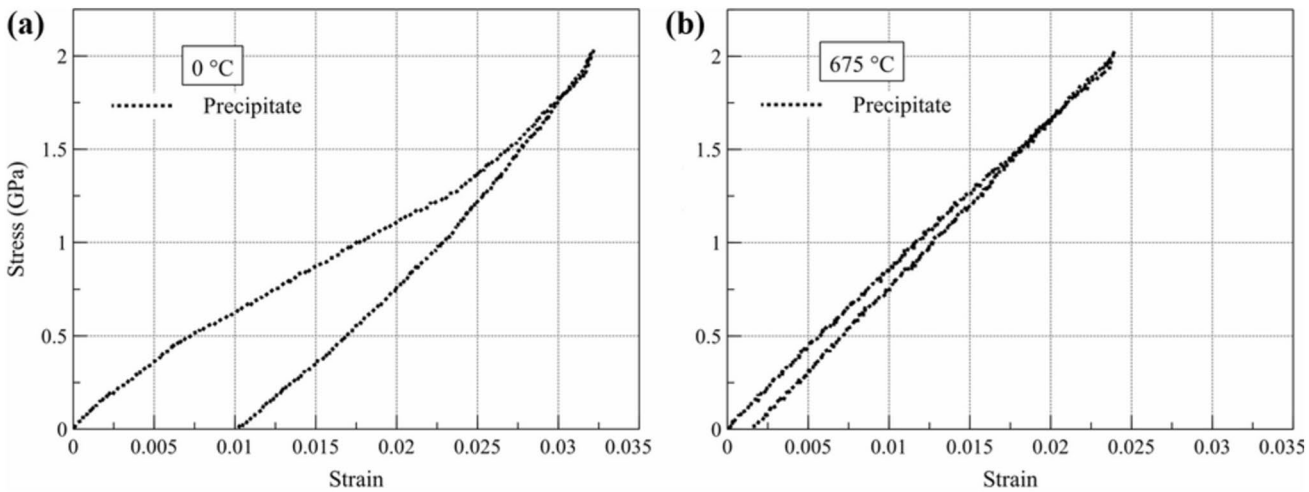

Fig. 4 Stress–strain response of solely precipitate model subjected to compressive load: **a** 0 °C, and **b** 675 °C

elastic response was observed at 675 °C, reaching a maximum strain of 0.024 (Fig. 4b).

The compressive stress–strain response of the NiTiHf models with and without precipitate along the [100] crystallographic direction and at martensitic and superelastic temperatures are presented in Fig. 5a and b, respectively. A martensitic behavior with residual strain at the end of unloading, can be observed for all the models at 0 °C in Fig. 5a. The single-precipitate and multi-precipitate models exhibit higher stress plateaus and maximum strains (under 2 GPa of stress) compared to the precipitate-free model. Although, previous research suggest that the H-phase precipitates are fully coherent with the austenitic matrix [26], after cooling the model to a martensitic temperature (i.e., 0 °C), this coherency between the H-phase precipitates and the matrix becomes disrupted due to the transformation strains. Because of the presence of H-phase precipitates, the martensitic matrix undergoes adjustments to accommodate the non-transforming particles, and this accommodation results in higher levels of strain. In Fig. 6a, the loss of coherency can be observed, where the models are characterized by Ovito's defect mesh analysis. This algorithm identifies those parts of the model that the atomic arrangement does not resemble a perfect crystal. Accordingly, insets (I) and (III) show the defect mesh (precipitate surface) of the single-precipitate and multi-precipitate models before equilibration, while insets (II) and (IV) represent the defect mesh after equilibration at martensitic temperature. It can be seen how the precipitates' surface became uneven and rough, which is the indication of coherency loss between precipitate and the matrix.

Figure 5b presents the superelastic stress–strain curves of the models loaded along [100] direction at the temperature of A_f+50 °C. During the loading phase, the austenitic alloys initially experienced elastic deformation. The stress-induced phase transformation was triggered around 0.025 strain in all the models. As the loading continued, the models underwent some transformation strains, characterized by a plateau

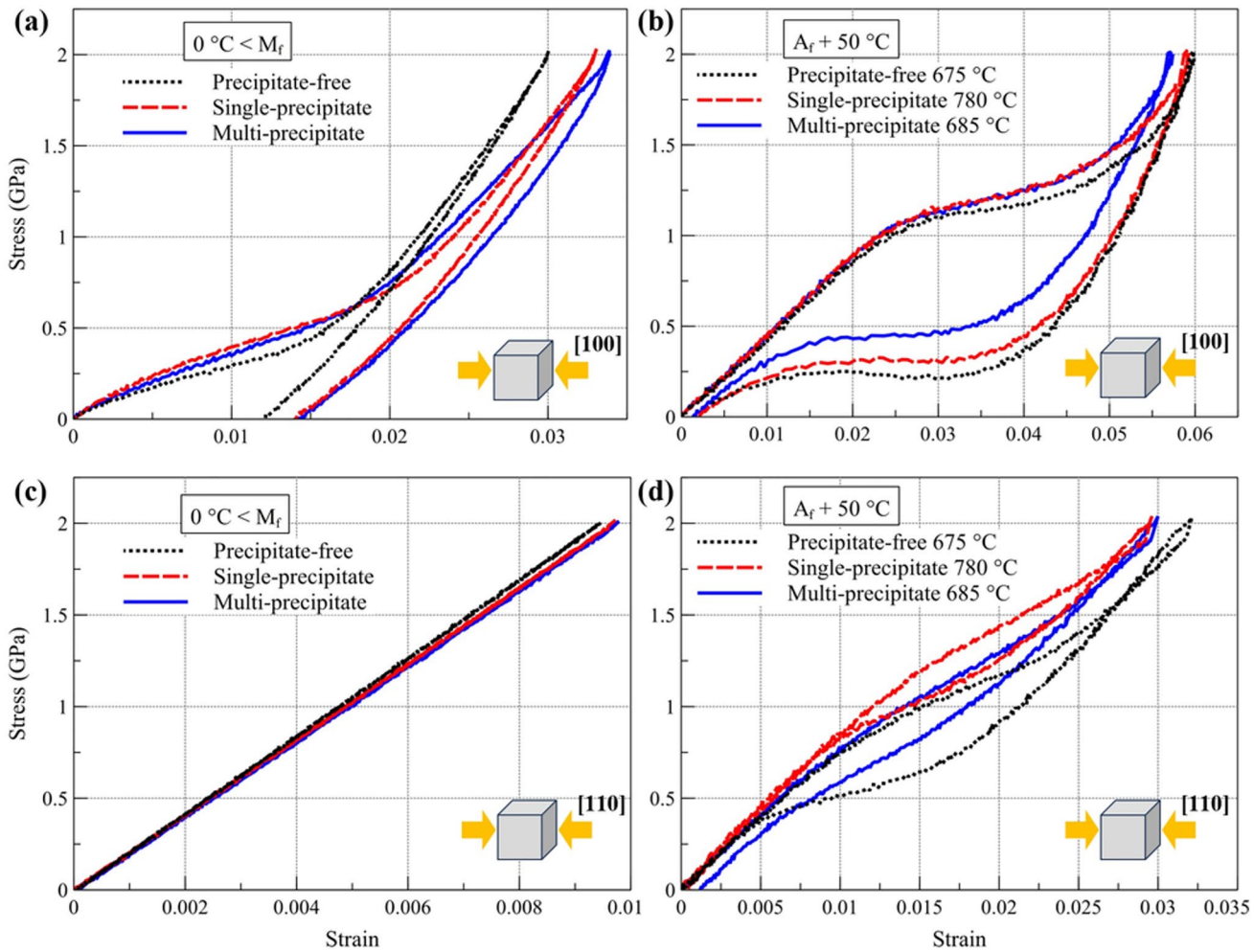

Fig. 5 Stress–strain response of the models subjected to compressive load along: **a** [100] direction at 0 °C, **b** [100] direction at A_f+50 °C, **c** [110] direction at 0 °C and **d** [110] direction at A_f+50 °C

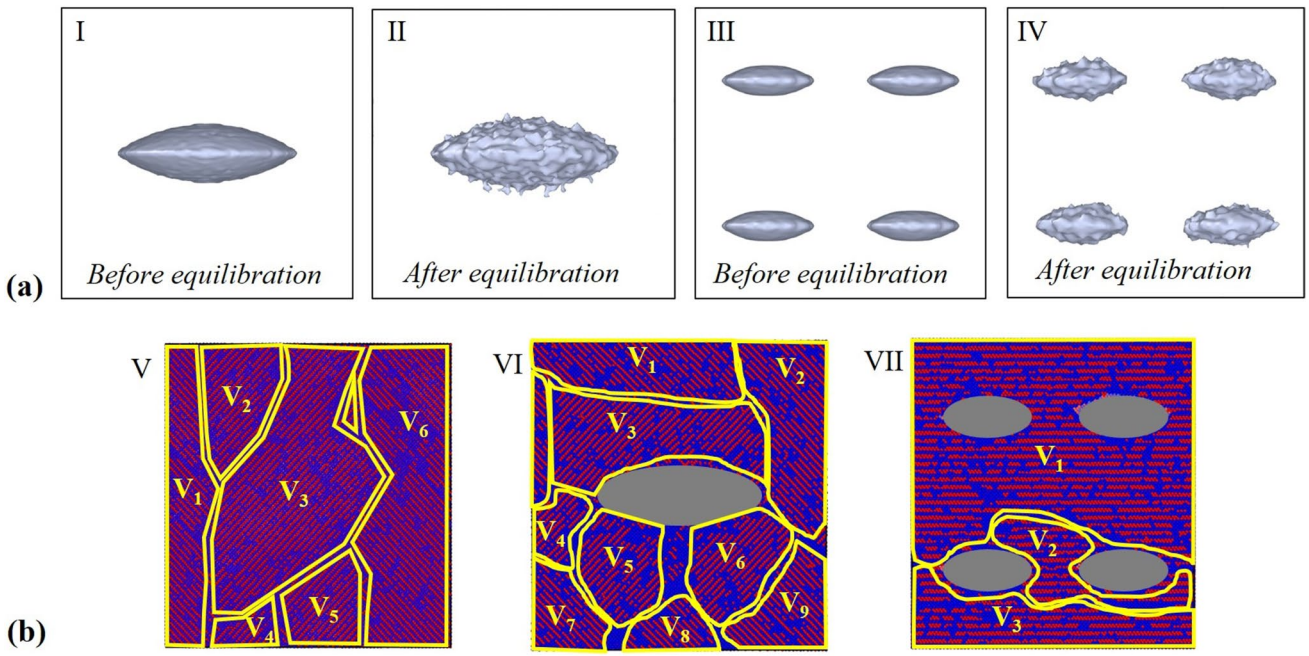

Fig. 6 **a** Coherency of precipitates before and after equilibration at 0 °C, **b** formed martensite variants in single- and multi-precipitate models at $A_f + 50$ °C

stage observed in the stress–strain curves. The superelastic stress–strain response observed in the multi-precipitate model, exhibited a reduction in the energy dissipation capacity (i.e., reduction in the size of hysteresis loop). Such a reduction in the size of the hysteresis loop can be favorable for higher fatigue resistance [38, 39]. Additionally, the transformation strain and maximum strain in the multi-precipitate model were lower compared to the other models since it is more challenging to select and grow martensite variants at the presence of many precipitates. Visualization of different martensite variants formed in the precipitate-free, single- and multi-precipitate models are presented in Fig. 6b. The annotation of variants was based on the distortion of each area compared to the original structure. As compared in the insets (VI) and (VII), the single-precipitate model exhibits more types of variants during stress-induced phase transformation.

Previous studies have highlighted the substantial influence of crystallographic orientation on the superelastic and martensitic behavior of Ni-rich NiTi alloys [28, 40–42]. In order to investigate the direction-dependence of these responses in NiTiHf and the impact of H-phase precipitates on them, a compressive load was applied along [110] direction (as opposed to previous case which was loaded along [100] direction) on the precipitated and precipitate-free models. Similar to [100] direction, the models were subjected to load at 0 °C and $A_f + 50$ °C. Figure 5c shows the stress–strain response of all the models at 0 °C. Both precipitated models and the precipitate-free model exhibited elastic behavior along [110] direction without any phase transformation, unlike the loading along [100] direction. It has been reported that in NiTi, grains orientated in [110] direction inhibit the stress-induced phase transformation and detwinning [43, 44]. The elastic behavior of all models in Fig. 5c can be attributed to the same reasoning since the models are at martensitic temperature, and under the applied load, they cannot transform from twinned to detwinned martensite. As can be seen in Fig. 5d, the stress–strain response of models at $A_f + 50$ °C was different from [100] direction. In models loaded along [110] direction, the maximum strain achieved was slightly over 0.03, whereas in the [100] direction, the maximum strain was twice as large. Additionally, the energy dissipation in [110] direction was considerably lower compared to [100] direction. Again, the martensitic transformation was hindered due to the crystallographic orientation leading to smaller transformation strains compared to [100] case. Furthermore, the single-precipitate and multi-precipitate models showed higher stress plateaus compared to precipitate-free model, similar to [100] direction.

Conclusions

In this study, MD simulations were employed on Ni-rich NiTiHf to investigate the effect of H-phase precipitates on the temperature- and stress-induced phase transformations.

Three scenarios were considered for the simulations of the alloy: containing a single large precipitate, multiple fine precipitates and no precipitate. Calculation of the TTs of the models indicated higher austenite start and finish temperatures for the models with precipitate(s), which was attributed to the smaller number of twinning planes in these models, that can act as nucleation sites during the reverse phase transformation leading to higher A_s and A_f. By applying a compressive load, the precipitated models exhibited larger transformation strains at martensitic temperature, as a result of disruption of coherency between the precipitate and the matrix at low temperatures, which causes the matrix to undergo adjustments to accommodate the non-transforming precipitate leading to larger transformation strains. Finally, by subjecting the models to the same compressive load along [110] crystallographic orientation, it was found that the maximum strain and energy dissipation are significantly smaller than the models that were subjected to the load along [100] direction.

References

1. Firstov GS, Van Humbeeck J, Koval YN (2006) High temperature shape memory alloys problems and prospects. J Intell Mater Syst Struct 17(12):1041–1047
2. Otsuka K, Wayman CM (1999) Shape memory materials, Cambridge University Press
3. Ma J, Karaman I, Noebe RD (2010) High temperature shape memory alloys. Int Mater Rev 55(5):257–315
4. Kockar B, Karaman I, Kim JI, Chumlyakov Y (2006) A method to enhance cyclic reversibility of NiTiHf high temperature shape memory alloys. Scr Mater 54(12):2203–2208
5. Meng XL, Zheng YF, Wang Z, Zhao LC (2000) Effect of aging on the phase transformation and mechanical behavior of $Ti_{36}Ni_{49}Hf_{15}$ high temperature shape memory alloy. Scr Mater 42(4):341–348
6. Ataollahi S (2023) Developing a new interatomic potential and atomistic study of NiTiHf, Ph.D. Dissertation, University of Tennessee at Chattanooga
7. Saghaian SM (2015) Shape memory behavior of single crystal and polycrystalline Ni-rich NiTiHf high temperature shape memory alloys, University of Kentucky
8. Khalil-Allafi J, Dlouhy A, Eggeler G (2002) Ni4Ti3-precipitation during aging of NiTi shape memory alloys and its influence on martensitic phase transformations. Acta Mater 50(17):4255–4274
9. Sehitoglu H, Canadinc D, Zhang X, Kotil T, Karaman I, Gall K, Maier H, Chumlyakov Y (2000) Overview of shape memory single crystals. Acta Mater 48(13):3311–3326
10. Ataollahi S, Mahtabi MJ (2023) An investigation of the growth of fatigue cracks in single crystal superelastic NiTi under high strain level using molecular dynamics simulations. Arab J Sci Eng. https://doi.org/10.1007/s13369-023-08460-x
11. Monroe JA, Karaman I, Lagoudas DC, Bigelow G, Noebe RD, Padula S (2011) Determining recoverable and irrecoverable contributions to accumulated strain in a NiTiPd high-temperature shape memory alloy during thermomechanical cycling. Scr Mater 65(2):123–126
12. Stebner AP, Bigelow GS, Yang J, Shukla DP, Saghaian SM, Rogers R, Garg A, Karaca HE, Chumlyakov Y, Bhattacharya K, Noebe RD (2014) Transformation strains and temperatures of a nickel–titanium–hafnium high temperature shape memory alloy. Acta Mater 76:40–53
13. Evirgen A, Karaman I, Noebe RD, Santamarta R, Pons J (2013) Effect of precipitation on the microstructure and the shape memory response of the $Ni_{50.3}Ti_{29.7}Zr_{20}$ high temperature shape memory alloy. Scr Mater 69(5):354–357
14. Benafan O, Moholt MR, Bass M, Mabe JH, Nicholson DE, Calkins FT (2019) Recent advancements in rotary shape memory alloy actuators for aeronautics. Shap Mem Superelasticity 5(4):415–428
15. Benafan O, Bigelow GS, Garg A, Noebe RD, Gaydosh DJ, Rogers RB (2021) Processing and scalability of NiTiHf high-temperature shape memory alloys. Shap Mem Superelasticity 7(1):109–165
16. Calkins FT, Fassmann AW, Vijgen PM, Nicholson DE, Bass MA, Benafan O, Gaydosh DJ, Bigelow GS, Noebe RD (2020) Shape memory alloy actuated vortex generators: shape memory alloy reconfigurable technology-vortex generators (SMART-VG) can reduce fuel consumption and improve aircraft efficiency. Adv Mater Process 178:60 (**in English**)
17. Sehitoglu H, Wu Y, Patriarca L, Li G, Ojha A, Zhang S, Chumlyakov Y, Nishida M (2017) Superelasticity and shape memory behavior of NiTiHf alloys. Shap Mem Superelasticity 3(2):168–187
18. König D, Zarnetta R, Savan A, Brunken H, Ludwig A (2011) Phase transformation, structural and functional fatigue properties of Ti–Ni–Hf shape memory thin films. Acta Mater 59:3267–3275
19. Thoma PE, Boehm JJ (1999) Effect of composition on the amount of second phase and transformation temperatures of NixTi90−xHf10 shape memory alloys. Mater Sci Eng A 273–275:385–389
20. Tong Y, Chen F, Tian B, Li L, Zheng Y (2009) Microstructure and martensitic transformation of Ti49Ni51−xHfx high temperature shape memory alloys. Mater Lett 63(21):1869–1871
21. Meng XL, Cai W, Chen F, Zhao LC (2006) Effect of aging on martensitic transformation and microstructure in Ni-rich TiNiHf shape memory alloy. Scripta Mater 54(9):1599–1604
22. Han XD, Wang R, Zhang Z, Yang DZ (1998) A new precipitate phase in a TiNiHf high temperature shape memory alloy. Acta Mater 46(1):273–281
23. Yang F, Coughlin DR, Phillips PJ, Yang L, Devaraj A, Kovarik L, Noebe RD, Mills MJ (2013) Structure analysis of a precipitate phase in an Ni-rich high-temperature NiTiHf shape memory alloy. Acta Mater 61(9):3335–3346
24. Coughlin DR, Casalena L, Yang F, Noebe RD, Mills MJ (2016) Microstructure–property relationships in a high-strength 51Ni–29Ti–20Hf shape memory alloy. J Mater Sci 51(2):766–778
25. Prasher M, Sen D (2014) Influence of aging on phase transformation and microstructure of $Ni_{50.3}Ti_{29.7}Hf_{20}$ high temperature shape memory alloy. J Alloys Compds 615:469–474
26. Santamarta R, Arróyave R, Pons J, Evirgen A, Karaman I, Karaca HE, Noebe RD (2013) TEM study of structural and

microstructural characteristics of a precipitate phase in Ni-rich Ni–Ti–Hf and Ni–Ti–Zr shape memory alloys. Acta Mater 61(16):6191–6206
27. Jung J, Ghosh G, Isheim D, Olson GB (2003) Precipitation of heusler phase (Ni_2TiAl) from B2-TiNi in Ni–Ti–Al and Ni–Ti–Al–X (X=Hf, Zr) alloys. Metall and Mater Trans A 34(6):1221–1235
28. Ataollahi S, Mahtabi MJ (2021) Effects of precipitate on the phase transformation of single-crystal NiTi alloy under thermal and mechanical loads: a molecular dynamics study. Mater Today Commun 29:102859
29. Ataollahi S, Mahtabi MJ (2023) An interatomic potential for ternary NiTiHf shape memory alloys based on modified embedded atom method. Comput Mater Sci 227:112278
30. Thompson AP, Aktulga HM, Berger R, Bolintineanu DS, Brown WM, Crozier PS, Veld PJ, Kohlmeyer A, Moore SG, Nguyen TD, Shan R, Stevens MJ, Tranchida J, Trott C, Plimpton SJ (2022) LAMMPS—a flexible simulation tool for particle-based materials modeling at the atomic, meso, and continuum scales. Comput Phys Commun 271:108171
31. Stukowski A (2009) Visualization and analysis of atomistic simulation data with OVITO–the open visualization tool. Modell Simul Mater Sci Eng 18(1):015012
32. Hirel P (2015) Atomsk: a tool for manipulating and converting atomic data files. Comput Phys Commun 197:212–219
33. Evirgen A, Pons J, Karaman I, Santamarta R, Noebe RD (2018) H-Phase precipitation and martensitic transformation in Ni-rich Ni–Ti–Hf and Ni–Ti–Zr high-temperature shape memory alloys. Shape Memory Superelasticity 4(1):85–92
34. Zhu J, Wu H-H, Wu Y, Wang H, Zhang T, Xiao H, Wang Y, Shi S-Q (2021) Influence of Ni4Ti3 precipitation on martensitic transformations in NiTi shape memory alloy: R phase transformation. Acta Mater 207:116665
35. Karaca HE, Acar E, Tobe H, Saghaian SM (2014) NiTiHf-based shape memory alloys. Mater Sci Technol 30(13):1530–1544
36. Karaca HE, Saghaian SM, Ded G, Tobe H, Basaran B, Maier HJ, Noebe RD, Chumlyakov YI (2013) Effects of nanoprecipitation on the shape memory and material properties of an Ni-rich NiTiHf high temperature shape memory alloy. Acta Mater 61(19):7422–7431
37. Larsen PM, Schmidt S, Schiøtz J (2016) Robust structural identification via polyhedral template matching. Modell Simul Mater Sci Eng 24(5):055007
38. Mahtabi MJ, Shamsaei N (2017) Fatigue modeling for superelastic NiTi considering cyclic deformation and load ratio effects. Shap Mem Superelasticity 3:250–263 (**in English**)
39. Mahtabi MJ, Stone TW, Shamsaei N (2018) Load sequence effects and variable amplitude fatigue of superelastic NiTi. Int J Mech Sci 148:307–315
40. Ataollahi S, Mahtabi MJ (2021) A molecular dynamics study on the effect of precipitate on the phase transformation in NiTi, ReSEARCH Dialogues Conference proceedings. https://scholar.utc.edu/research-dialogues/2021/posters/2
41. Hamilton RF, Sehitoglu H, Chumlyakov Y, Maier HJ (2004) Stress dependence of the hysteresis in single crystal NiTi alloys. Acta Mater 52(11):3383–3402
42. Sehitoglu H, Jun J, Zhang X, Karaman I, Chumlyakov Y, Maier HJ, Gall K (2001) Shape memory and pseudoelastic behavior of 51.5%Ni–Ti single crystals in solutionized and overaged state. Acta Mater 49(17):3609–3620
43. Weafer FM, Bruzzi MS (2014) Influence of microstructure on the performance of nitinol: a computational analysis. J Mater Eng Perform 23(7):2539–2544
44. Gall K, Sehitoglu H, Chumlyakov YI, Kireeva IV (1999) Tension–compression asymmetry of the stress–strain response in aged single crystal and polycrystalline NiTi. Acta Mater 47(4):1203–1217